Article ID: 1006-8775(2019) 01-0114-15

DYNAMICAL PREDICTION OF WEST CHINA AUTUMN RAINFALL BY THE NCEP CLIMATE FORECAST SYSTEM

DONG Shao-rou (董少柔)[1], YANG Song (杨 崧)[1], ZHANG Tuan-tuan (张团团)[1], FENG Ye-rong (冯业荣)[2]
(1. School of Atmospheric Sciences and Guangdong Province Key Laboratory for Climate Change and Natural Disaster Studies, Sun Yat-sen University, Guangzhou 510275 China; 2. Guangzhou Institute of Tropical and Marine Meteorology/Guangdong Provincial Key Laboratory of Regional Numerical Weather Prediction, Guangzhou 510641 China)

Abstract: This study investigates the variation and prediction of the west China autumn rainfall (WCAR) and their associated atmospheric circulation features, focusing on the transitional stages of onset and demise of the WCAR. Output from the 45-day hindcast by the National Centers for Environmental Prediction (NCEP) Climate Forecast System version 2 (CFSv2) and several observational data sets are used. The onset of WCAR generally occurs at pentad 46 and decays at pentad 56, with heavy rainfall over the northwestern China and moderate rainfall over the south. Before that, southerly wind changes into southeasterly wind, accompanied by a westward expansion and intensification of the western Pacific subtropical high (WPSH), favoring rainfall over west China. On the other hand, during the decay of WCAR, a continental cold high develops and the WPSH weakens and shifts eastward, accompanied by a demise of southwest monsoon flow, leading to decay of rainfall over west China. The CFSv2 generally well captures the variation of WCAR owing to the high skill in capturing the associated atmospheric circulation, despite an overestimation of rainfall. This overestimation occurs at all time leads due to the overestimated low-level southerly wind. The CFSv2 can pinpoint the dates of onset and demise of WCAR at the leads up to 5 days and 40 days, respectively. The lower prediction skill for WCAR onset is due to the unrealistically predicted northerly wind anomaly over the lower branch of the Yangtze River and the underestimated movement of WPSH after lead time of 5 days.

Key words: west China autumn rainfall; NCEP CFSv2; prediction; predictable patterns
CLC number: P457.6 **Document code:** A
doi: 10.16555/j.1006-8775.2019.01.011

1 INTRODUCTION

The west China autumn rainfall (WCAR), characterized by continual rainfall, high moisture, and a lack of sunlight, is the second peak of rainfall in west China (Zhang[1]; Bai and Dong[2]; Yuan and Liu[3]). Its domain covers Sichuan, Chongqing, Guizhou, eastern and southern Gangsu, Guanzhong, southern Shaanxi, western Hunan and Hubei (Gao and Kuo[4]; Liang[5]). The WCAR is regarded as a special rainfall process in autumn, especially in September and October. Due to the influences of this last wet season over mainland China (Wang and Ding[6]; Yu et al.[7]) on agricultural production, geological hazards (e.g. debris flow and landslide), and autumn flood, numerous studies have been conducted to understand the cause and impact of the WCAR (Bao et al.[8]; Cai et al.[9]; Li et al.[10]; Liu et al.[11]) and monitor its variations (Wang et al.[12]).

Previous studies have investigated the variability of WCAR on different time scales. As a transitional phenomenon (Huang et al.[13]), WCAR is associated with the adjustment of atmospheric circulation from the summer pattern to the winter pattern in the Northern Hemisphere. On interannual time scale, Ren and Li [14] pointed out that WCAR amplified approximately every 5.5 years. Jiang et al. also found that WCAR exhibited an oscillation of about 6 years [15]. Wang et al. analyzed the relationship between WCAR and ENSO based on a 4-year cycle of WCAR [16]. Xu et al. indicated that both ENSO and the Indian Ocean Dipole (IOD) strongly influenced the interannual variability of WCAR[17]. In addition, WCAR also experiences strong interdecadal variability (Zhang[1]; Feng and Guo [18]; Zhao et al.[19]; Xue et al.[20]). WCAR shows a weakening tendency during the last 50 years in the 20th century and then strengthens again after the 21st century (Li et al.[10]; Liu et al.[11]; Jiang et al.[15]; Xue et al.[21]; Luo et al.[22]). The factors that contribute to WCAR variability are complex. The possible effects of the topography of west China[2], the intensity and position of the western Pacific subtropical high (WPSH), the East Asian jet stream (EAJS) coupled with the retreat of

Received 2018-01-16; **Revised** 2018-09-05; **Accepted** 2019-02-15
Foundation item: National Natural Science Foundation of China (41661144019); State Key Research Plan of China (2014CB953904); LASW State Key Laboratory Special Fund (2016LASW-B01)
Biography: DONG Shao-rou, Ph.D., primarily undertaking research on numerical simulation and urban climate.
Corresponding author: YANG Song, e-mail: yangsong3@mail.sysu.edu.cn

the Indian monsoon[4], the sea surface temperature (SST) in the tropical Pacific (Li et al.[10]; Wang et al.[16]; Wang et al.[23]), and the eastern heat source and snow cover of the Tibetan Plateau (Xue et al.[21]; Chen et al.[24]; Ai et al.[25]) have been discussed by previous studies.

Because various meteorological disasters are induced by WCAR, substantial effort has been devoted to simulate and predict the phenomenon (Shao et al.[26]; He[27]; Liu et al.[28]; Pan et al.[29]; Saha et al.[30]). The National Centers for Environmental Prediction (NCEP) Climate Forecast System (CFS) is a state-of-the-art operational climate forecast system, which shows reliable skills in climate prediction(Saha et al.[31]; Gao et al.[32]). As a fully coupled model, it not only provides the official forecast of the U.S. climate but also is an important source of information for global and regional climate prediction, such as ENSO, the Asian summer monsoon (Yang et al.[33]), the East Asian winter monsoon (Li and Yang [34]), and the rainfall patterns over the Indo-Pacific region and North America (Zuo et al.[35]; Kim et al.[36]). In 2011, the early version of the CFS was substituted by version 2 (CFSv2) and this modified version represents a substantial change to all aspects of the forecast system including model components, data assimilation system, and ensemble configuration (Zuo et al.[35]). The CFSv2 demonstrates improved skills in predicting large-scale monsoon circulation (Jiang et al.[37]), the Madden-Julian Oscillation (MJO) (Wang et al.[38]), extratropical climate (Gao et al.[39]), etc. Zhao and Yang [40, 41] explored the ability of the CFSv2 in predicting the early-season rainfall (ESR) over southern China and found that the ESR could be predicted by 2 weeks in advance. Like the ESR, the WCAR is also an important regional rainfall process that exerts influences on both human lives/properties and social-economic development. It is anticipated that the CFSv2 also possesses skills in simulating and predicting WCAR variations to various extents; however, these possible skills have never been assessed.

In this study, we evaluate the prediction skills of the CFSv2 for WCAR variations and their relationships with large-scale climate anomalies. The rest of this paper is organized as follows. Section 2 introduces the model output and observational data sets applied in this study. In section 3, the major features of the WCAR and associated atmospheric circulation predicted by the CFSv2 at 0-day lead are depicted, with a comparison against observations. Section 4 contains an assessment of the major features of predicted WCAR at different leads of time and the atmospheric circulation during the transitional periods before and after the WCAR. Finally, a summary of the results obtained and a further discussion are provided in section 5.

2 MODEL, DATA AND METHODS

The NCEP CFSv2, a fully coupled dynamical prediction system, consists of the NCEP Atmospheric Global Forecast System with T126 resolution in the horizontal and 64 sigma layers in the vertical as the atmospheric component. Its land and ocean components are the NCEP, Oregon State University (OSU), the Air Force, and the Hydrologic Research Laboratory land model and the Modular Ocean Model version 4.0 from the Geophysical Fluid Dynamics Laboratory of the National Oceanic and Atmospheric Administration (EK et al.[42]; Griffies et al.[43]; Moorshi et al.[44]), respectively. The output of rainfall, 850 hPa and 200 hPa winds, and 500 hPa geopotential height from the retrospective forecasts of 45-day integrations of the CFSv2 is used. The hindcast runs were initialized from every 0000 Coordinated Universal Time (UTC), 0600 UTC, 1200 UTC, and 1800 UTC cycle from 2000 to 2014. The longest lead time for a target day is 44 days. The 0-day lead represents that the model runs were initialized on the current day; the 1-day lead for the forecasts were initialized on the previous day; the 44-day lead were initialized 44 days ago. In this paper, pentad means are applied to daily data to remove the higher-frequency signals that may interfere with the determination of transitional date (Zhang et al.[45]). There are totally 73 pentads for each year from 1-5 January (the first pentad) to 27-31 December (the last pentad), with 29 February being omitted in the leap years. For convenience, LD0, LD1, LD2, …, and LD44 represent 0-day lead, 1-day lead, 2-day lead, …, and 44-day lead, respectively.

The observational data used comprise the daily precipitation with a horizontal resolution of 1° in both latitude and longitude from the Global Precipitation Climatology Project (GPCP) (Adler et al.[46]), winds with a horizontal resolution of 1° from the ECMWF/European Centre for Medium-range Weather Forecasts (Dee et al.[47]), and 500 hPa geopotential height with a horizontal resolution of 2.5° from the NCEP/National Center for Atmospheric Research (NCEP/NCAR) Reanalysis (Kalnay et al.[48]). Moreover, the precipitation from approximately 850 meteorological stations in China is used to confirm the reliability of the GPCP data and the simulating result from the model. In this study, the spatial domain of WCAR is defined as the region of 24.5-39.5°N /99.5-110.5°E.

3 PREDICTION OF WCAR IN LD0

3.1 *Major features in observation*

Figure 1a shows the climatological (2000-2014) rainfall in China from the 3rd pentad in August to the 3rd pentad in October (Kao and Kuo[4]; Yuan[49]). During this period, heavy rainfall is mainly over west China and the east coast of China (Fig. 1a). We have also analyzed the climatological rainfall in China during the same period, but from 1979 to 2014 using both station and GPCP data (figure not shown) and found that the features depicted by the two data sets are like those shown in Fig. 1a. According to previous studies[6, 14, 15, 18], we choose 99.5°E

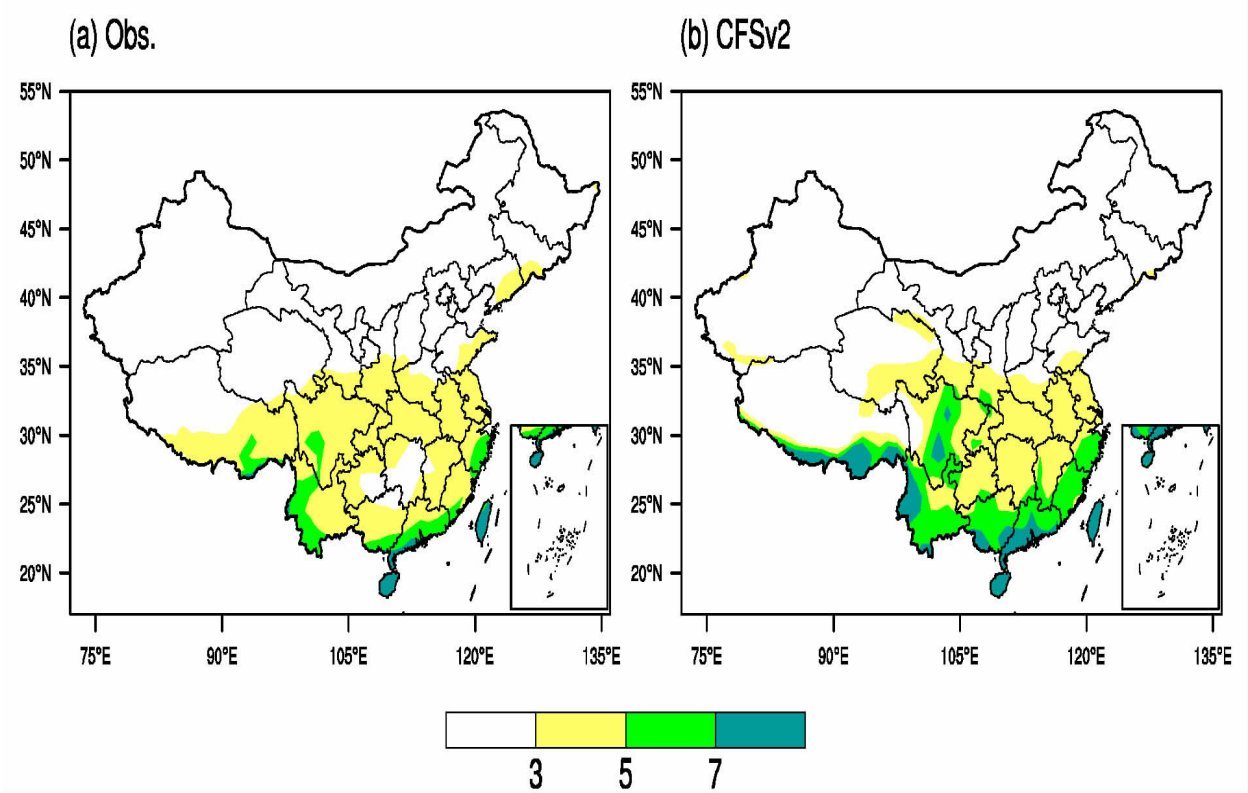

Figure 1. The WCAR (mm day^{-1}) averaged from pentad 3 in August to pentad 2 in October for (a) GPCP and (b) CFSv2 at LD0.

and 110.5° E to represent the west and east borders of WCAR, respectively.

Figure 2 shows the time-latitude cross-sections of climatological pentad-mean rainfall and 850 hPa winds along the longitudes of WCAR in observation. According to Fig.2a, the largest rainfall occurs during early June to late July due to the influence of summer monsoon circulation and rainfall decreases subsequently, followed by a secondary rainfall increase over west China in August. Rainfall reaches its secondary peak over northwestern China after pentad 46 and then decreases rapidly. The rainfall over southwestern China (25-29°N) experiences an earlier decrease at around pentad 46. These features are also shown by China station data, which reveals a smaller magnitude (Fig. 2c). Correspondingly, the low-level southerly wind changes to southeasterly wind from the north to the south at around pentad 46 and then the wind gradually weakens during October. This transitional feature and the weakening of southeasterly wind are associated with the movement of the WPSH, which will be discussed later.

To measure the overall change in rainfall when WCAR starts and ends, we define the time of WCAR onset and demise following several criteria. (1) The starting pentad is determined when the area-averaged rainfall first reaches its peak after pentad 43. (2) The ending pentad is determined when the area-averaged rainfall is below the annual mean but higher than that of the following pentad, and the rainfall of the following 6 pentads is all below the annual mean. Fig. 3 shows the climatological pentad-mean precipitation over west China, in which the black line represents observed precipitation. The rainfall displays strong sub-seasonal variations, with an annual mean of 2.22 mm per day. After the peak value in early summer, rainfall decreases; and then it increases and reaches a second peak in autumn. According to the definition, the WCAR starts at pentad 46 and ends at pentad 56. Similar features can also be seen from the station data (figure not shown). From above analysis, the WCAR can be regarded as a part of the continual process in which rainfall peaks in summer, weakens slightly afterwards, and increases again in late August before it decays finally.

The associated atmospheric circulations in observation are shown in the left panels of Fig. 4. Before the WCAR occurs (at pentads 42-44), the subtropical ridge line is located at around 32° N; the convergence zone over India is at its northernmost position; strong southwesterly wind affects west China. Southerly wind prevails in the south of the Yangtze River. When the WCAR occurs (at pentad 46), several changes are apparent. The transformation of winds from southerly flow to easterly flow over northern central China is associated with an obvious anticyclone over the Shandong Peninsula, and a westward extension of strengthened subtropical high is accompanied by a change from southerly wind to southeasterly wind over southern central China. This transition of winds over southern

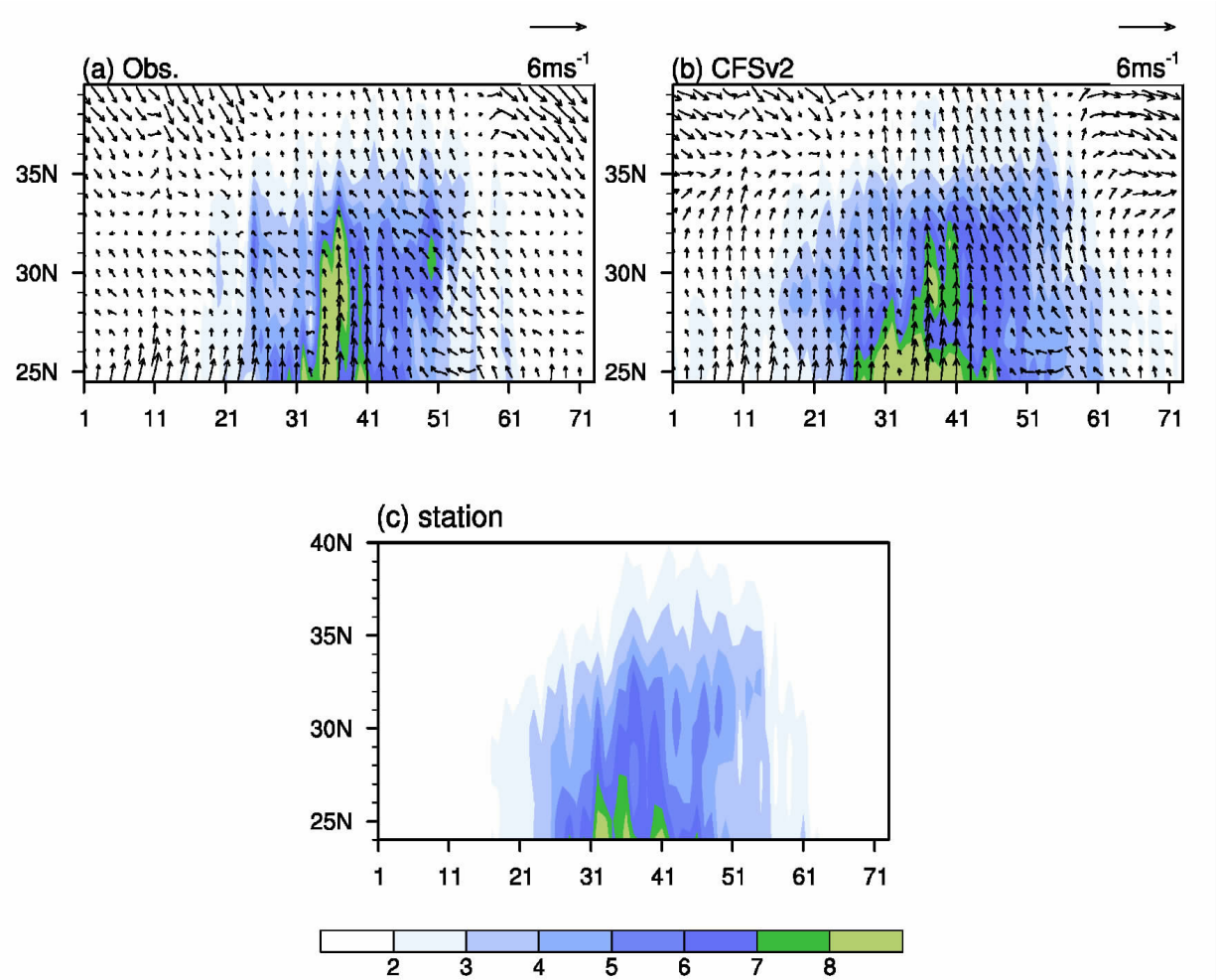

Figure 2. Time-latitude cross-sections of climatological pentad-mean precipitation (shaded areas; mm/day) and 850 hPa winds (vectors; m/s) along longitudes 99.5°-110.5°E from pentad 1 to pentad 73 (*x*-coordinate) for (a) GPCP and the NCEP-NCAR reanalysis, (b) CFSv2 LD0 prediction, and (c) gauge precipitation of meteorological stations.

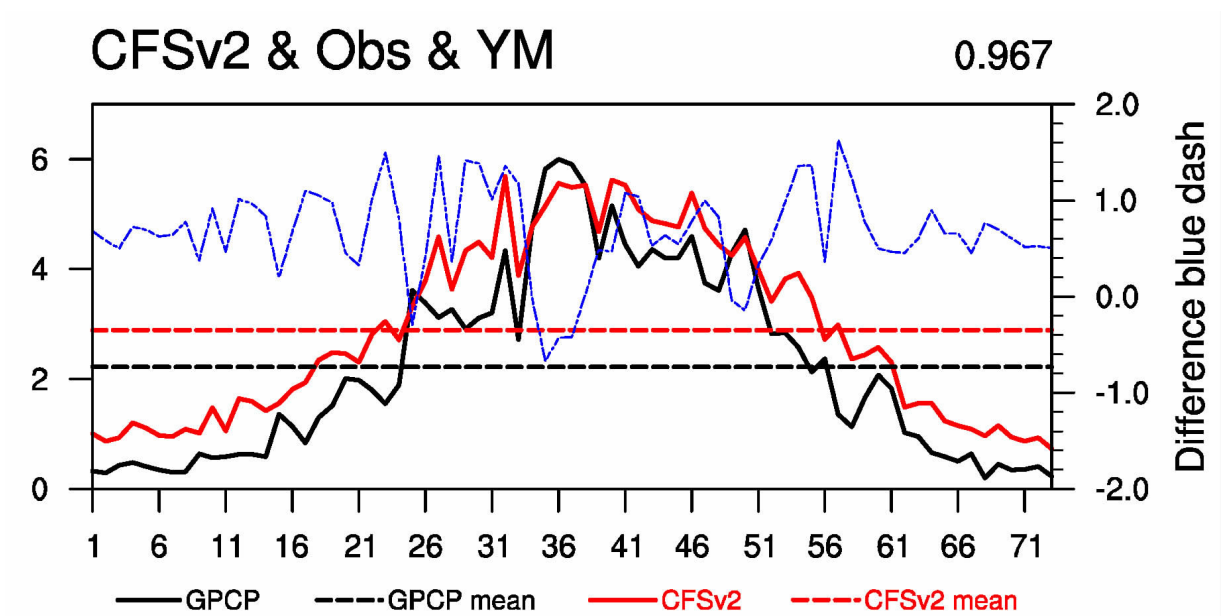

Figure 3. Climatological pentad-mean precipitation (mm/day) averaged over west China (24.5°-39.5°N, 99.5°-110.5°E) for GPCP (black solid line), CFSv2 LD0 (red solid line), and their difference (blue dashed line, coordinate on the right). The horizontal black dashed line and red dashed line indicate the annual mean values for observation and CFSv2 LD0, respectively.

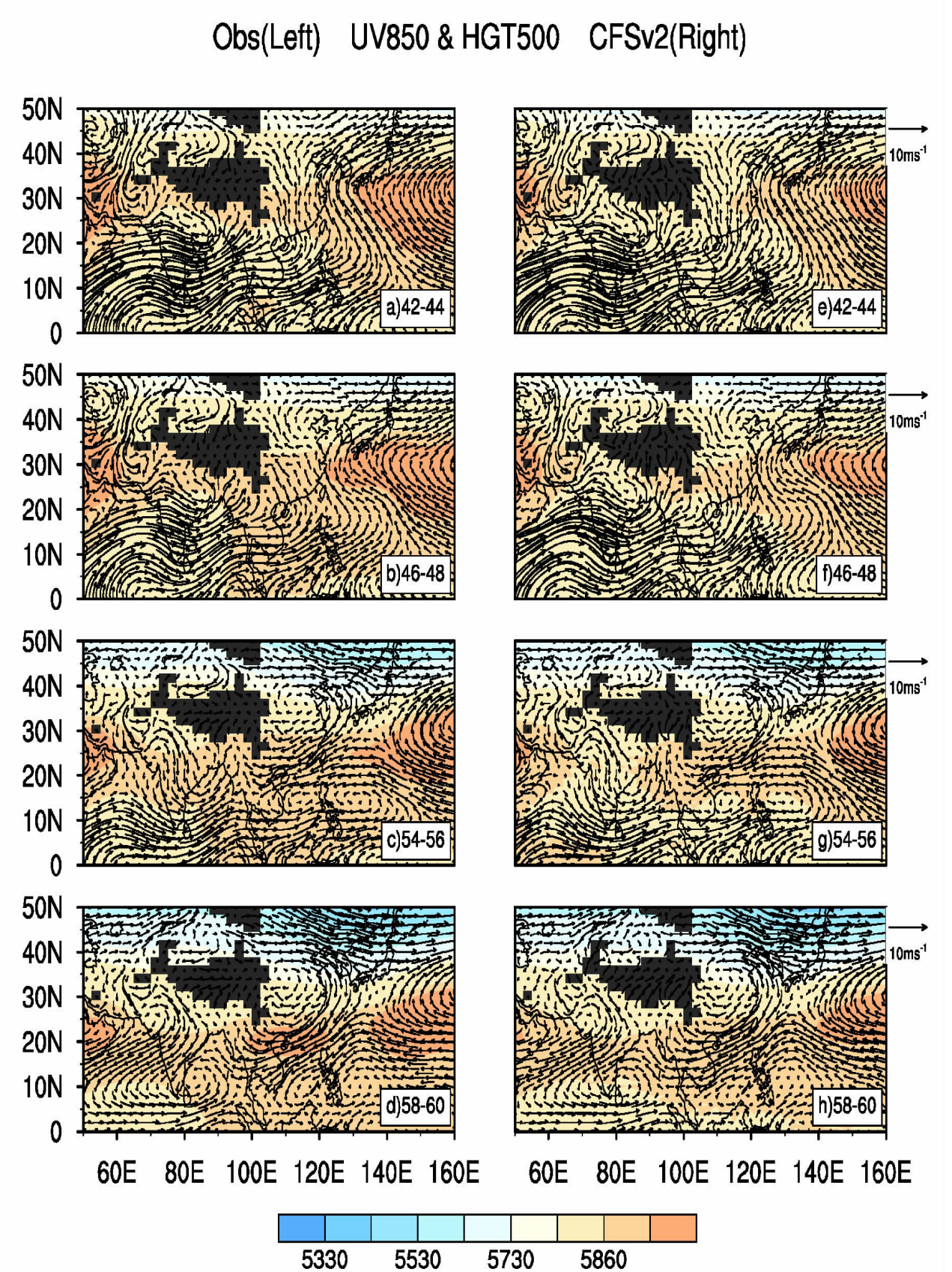

Figure 4. Climatological 3-pentad mean 850 hPa winds (vectors; m/s) and 500 hPa geopotential height (shaded areas; meter) for observation (left panels) and CFSv2 LD0 (right panels).

central China (Fig. 4b) in the beginning of WCAR has facilitated the transport of moisture from the East China Sea to west China. It should be noted that the southwest monsoon also favors rainfall over west China. As a result, rainfall reaches its second peak over west China (i.e. the WCAR). In pentads 54-56 (before WCAR decays), East Asia is controlled by a continental cold high and the subtropical high weakens and shifts eastward, which contribute to the decrease in rainfall over west China, despite that the weakening southwest monsoon is still in favor of rainfall in west China. In pentads 58-60, southwest monsoon flow is prohibited from entering west China due to the development of the continental cold high, which cuts off moisture supply thereby ending the WCAR.

3.2 *Prediction in LD0*

As in Fig. 1b, the NCEP CFSv2 shows generally good skills in simulating the climatological spatial distribution of WCAR except an overestimation especially for the Sichuan Basin. Fig. 2b, which shows the time-latitude cross-sections of climatological pentad-mean precipitation and 850 hPa winds along the longitudes of WCAR at LD0, indicates that the model captures the major features observed (Fig. 2a and Fig. 2c), but overestimates the southwestern China rainfall and underestimates the northwestern China rainfall, resulting in a smaller northern-southern difference in rainfall compared with observed. The associated transition and decay of the low-level winds are also well simulated, except an overestimation in the magnitude. These stronger-than-observed low-level winds provide more moisture and contribute to the overestimation of WCAR.

Figure 3, in which the red solid line and the red dashed line respectively represent the climatological pentad-mean and the yearly-mean rainfall of west China at LD0, shows that the yearly-mean rainfall in the model (red dashed line) reaches 2.89 mm per day, higher than the observed value of 0.67 mm per day. The CFSv2 well captures the sub-seasonal variation of rainfall over west China, with a correlation coefficient of 0.967 between the observation and the model through the whole year, despite an overall overestimation of rainfall. It well simulates the onset and demise of WCAR, owing to its high skill in capturing the features of atmospheric circulation as discussed above.

Compared with the observational features shown in the left panels of Fig. 4, the characteristics of atmospheric circulation are well simulated by the CFSv2 (the right panels of Fig. 4), including the location of the subtropical high during the WCAR period, the transition of low-level winds when the WCAR occurs, and the development of the continental cold high as the WCAR decays. However, the subtropical high is weaker than observed, leading to weaker southeasterly wind over China. The westward extension of the underestimated subtropical high is also limited so that cold air cannot be trapped in the western or northern Sichuan Basin[8-10], thus reducing the rainfall over northwestern China. Additionally, in the model, southwestern China such as Guizhou Province is under the control of low pressure system at the edge of the subtropical high, yielding more rainfall over southwestern China due to strong upward movement when the complex topography is taken into account[1]. Therefore, the gradient of observed rainfall during the early stage of WCAR is underestimated by the model due to the underestimation and overestimation of rainfall over the northwestern and southwestern China, respectively.

The model well captures the development of continental cold high near the end of WCAR, and successfully simulates the transition of atmospheric circulation from the summer type to the winter type. The model can generally capture the transform from easterly wind to westerly wind at the higher levels over northwestern China at the beginning of WCAR[4], the high-level divergence and low-level convergence over west China during the WCAR, the withdrawal of the Indian monsoon, and the appearance of westerly jet stream over the Sichuan Basin in addition to the large convergence at 200 hPa level during the end of WCAR[4] (figures not shown) are all generally captured by the model (figures not shown). These good skills all contribute to the model's good performance in capturing the onset and demise dates of WCAR.

4 PREDICTION IN DIFFERENT LEADS

4.1 *Prediction of WCAR in different leads*

Figure 5 shows the pentad-mean precipitation predicted by the CFSv2 of different leads at LD1, LD5, LD10, …, and LD40. Overall overestimations of rainfall and underestimations of the north-to-south gradient of rainfall can be seen at all leads of time. The difference in 850 hPa winds between model and observation exhibits southerly anomalies over southern China, causing overestimated rainfall (figures not shown). This overestimation weakens with lead time, which can be ascribed to the growing underestimation of the subtropical high with increasing leads (figures not shown). The model well captures the southeasterly flow associated with the gradually westward shift of the WPSH at all leads, despite the exaggerated southerly wind component.

From Fig. 6, the magnitude of overestimated rainfall over west China decreases as lead time increases. After the lead of 2 weeks, the bias of annual mean rainfall between model and observation drops from 1.29 mm to 0.91 mm. Within the lead of two weeks, the overestimation of WCAR (from pentad 46 to pentad 56) is more apparent than that in the longer leads, which can also be seen from the root-mean-square errors (RMSE) for the WCAR period at different leads. Fig. 6 also shows that the prediction errors (blue line) are mainly contributed by the overestimation of rainfall during the

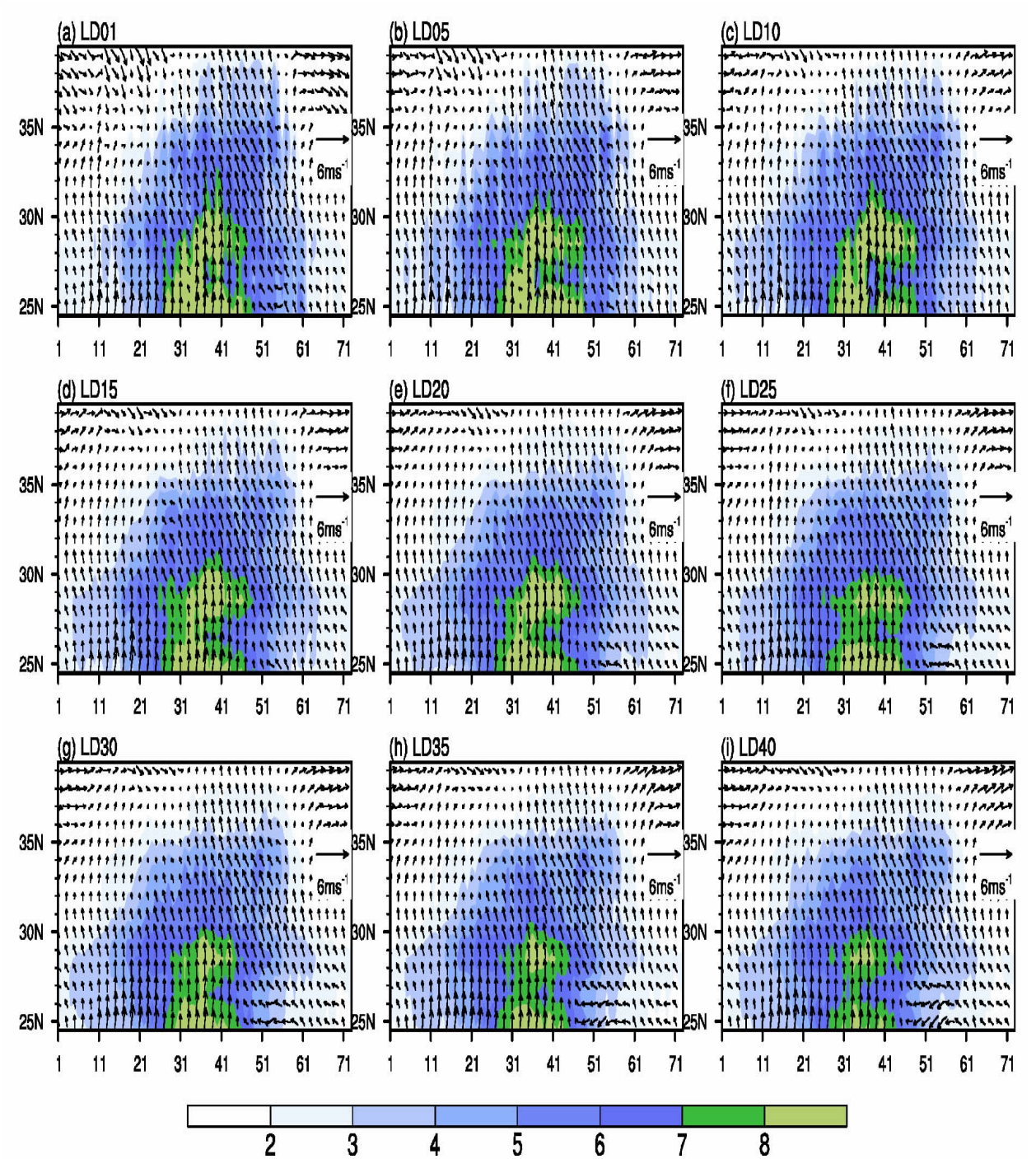

Figure 5. Same as Fig. 2b, but for LD1, LD5, LD10, LD15, LD20, LD25, LD30, LD35, and LD40.

late stage of WCAR. The correlation coefficient for the WCAR period remains surprisingly high at all leads; that is, the CFSv2 can well mimic the climatological variation of WCAR even at long leads. In addition, the model captures the onset and the demise of WCAR up to 5 days and 40 days, respectively. An analysis of the area-weighted mean convergence of the low-level winds also shows features that are consistent with those discussed above (figure not shown).

Previous studies have shown that the position and strength of the East Asian jet stream (EAJS) may influence rainfall variations not only in East Asia (Xu and Lin[50]) but also in west China (Ai et al.[25]; Yang et al.[51]). In observation (left panels of Fig. 7), the maximum center of high-level zonal wind shifts eastward during WCAR, with a decay of large-scale anticyclone over the Tibetan Plateau. The CFSv2 well predicts the position and strength of the EAJS as well as the high-level atmospheric circulation at all leads (only LD1 is shown), explaining why the model possesses good skills in predicting the variation of WCAR even at long leads of time as mentioned in Fig. 6.

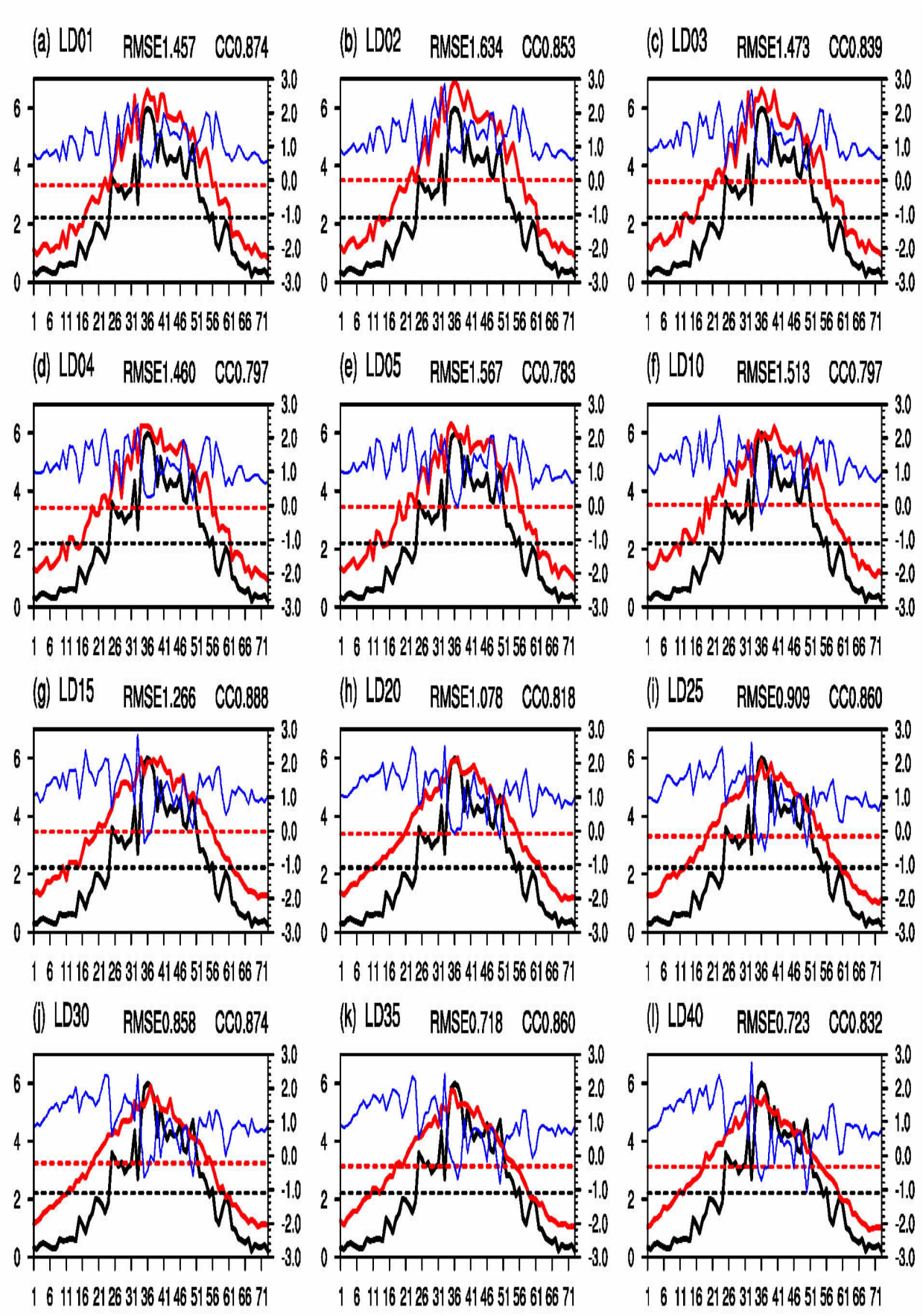

Figure 6. Same as Fig. 3, but for different leads of time. RMSE and correlation coefficient are counted from pentad 46 to pentad 56 between observation and CFSv2 at certain leads of time.

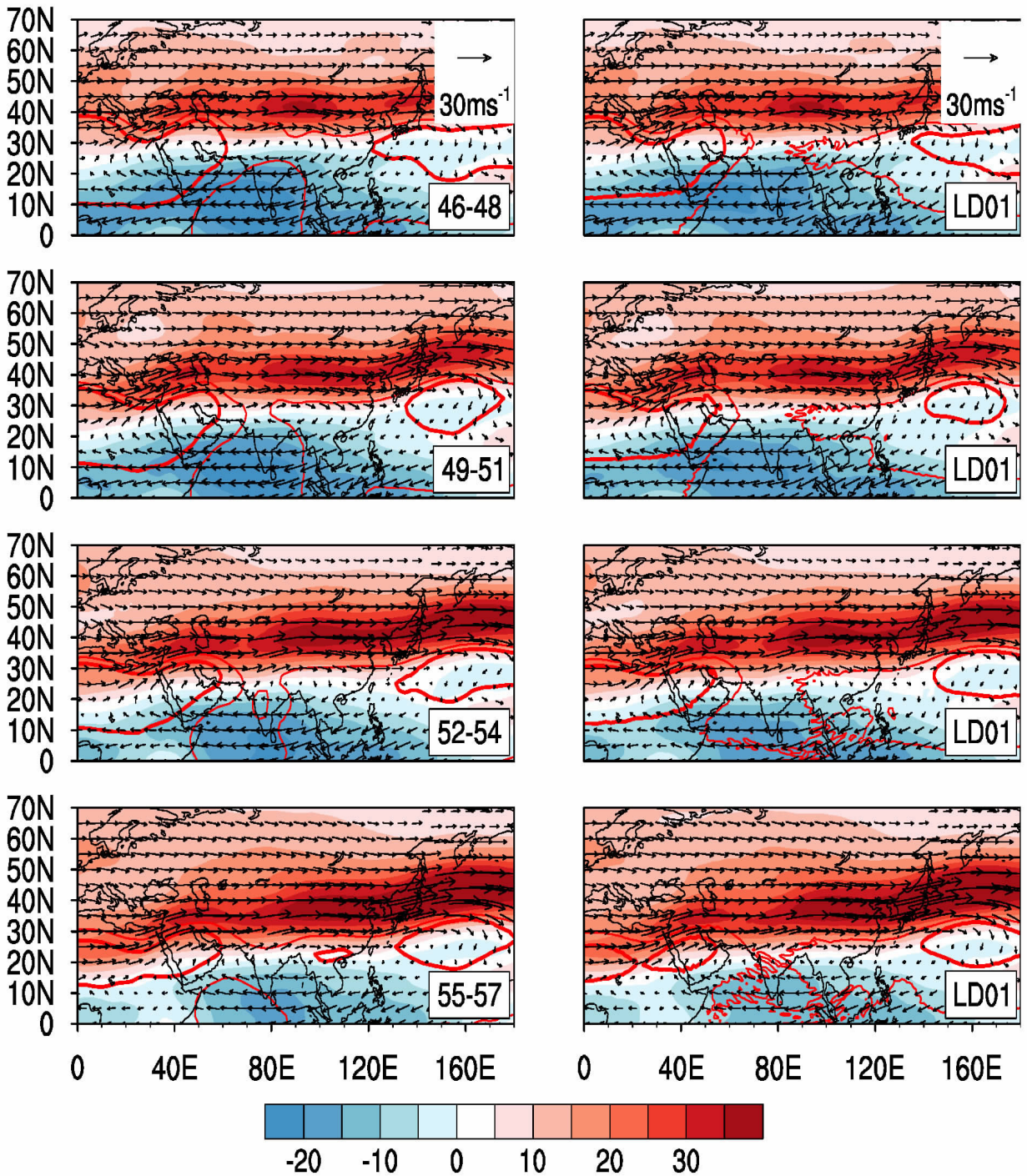

Figure 7. Climatological 3-pentad mean 200 hPa winds (vectors; m/s), 5880&5860 geopotential height (contours; meter), and U200 (shaded areas; m/s) for observation (left panels) and CFSv2 LD1 (right panels).

4.2 *Prediction of the onset and demise of WCAR in different leads*

Southerly wind is replaced by southeasterly flow when the WCAR starts, implying an adjustment of atmospheric circulation as shown in Fig. 2a and Fig. 4a-b. The question is how the associated atmospheric circulations at different levels change during the transitions of onset and demise of the WCAR and to what extent the model captures them.

Figure 8 manifests that southerly winds weaken (northerly wind anomalies) over west China, central China, and south China during the onset of WCAR in observation. In the CFSv2, northerly wind anomalies occur not only over the above-mentioned areas but also over the lower branch of the Yangtze River and to the south of the Yangtze River (Fig. 8, LD5-LD20), implying the decay of predicted southerly winds over/near the Yangtze River areas after LD5. As shown in previous

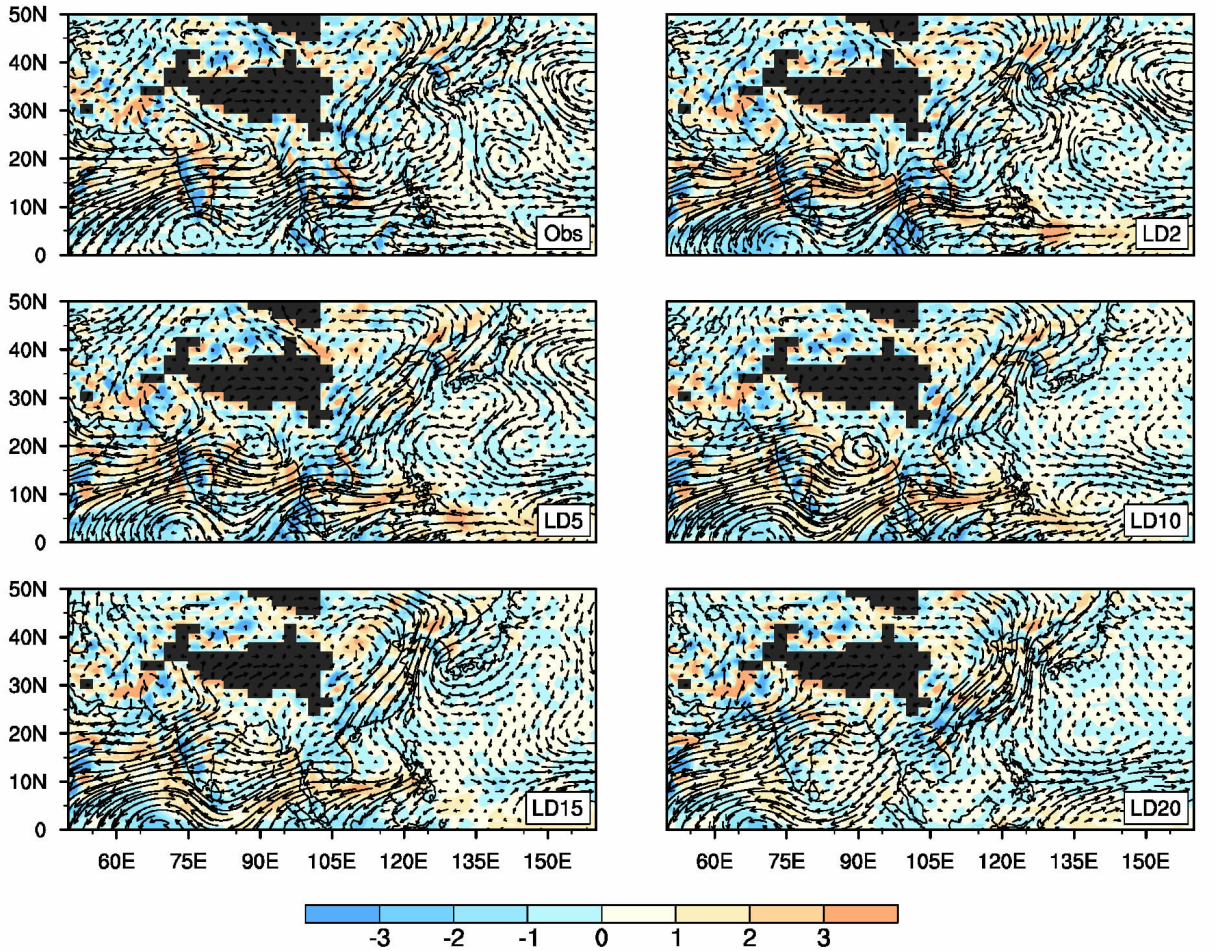

Figure 8. Differences between the mean of pentads 42-44 and the mean of pentads 46-48 for 850 hPa winds (vectors; m/s) and $\nabla \cdot V$h.

studies, this southerly flow comes from the South China Sea monsoon (Yeh et al.[52]; Chen et al.[52]; Zhang et al.[53]) and the subtropical summer monsoon, and it encounters the southwesterly flow from the Indian monsoon over west China to trigger the WCAR[3]. The exaggeration of northerly anomaly before WCAR onset in the model after LD5 inhibits the transport of moisture so that the model cannot capture the start date of WCAR after LD5. However, the transformation of associated general circulation near the end of WCAR is generally well captured, explaining the good skill of the model in capturing the demise of WCAR with a long lead up to 40 days (figure not shown).

At the middle troposphere, the change in the subtropical high before and after the onset of WCAR can be seen from the contours with different colors. In observation, the high strengthens near the start of WCAR (Fig. 9, Obs). The model well captures this feature before LD5 but it fails in catching this variation after LD10. The subtropical high can not only facilitate the transformation from southerly flow to southeasterly flow over the lower branch of the Yangtze River but also deepen the India-Burma trough to foster another important moisture contributor, the southwesterly flow over South Asia. Thus, the rainfall triggered by these two main flows during WCAR is closely associated with the westward extension of the subtropical high. The failure in capturing the strengthening high should be responsible for the poor skill of the model in predicting the onset of WCAR after LD5. On the other hand, the model well captures the weakening of the WPSH before the demise of WCAR, contributing to higher prediction skill for WCAR demise (figure not shown).

The prediction skill of the position and magnitude of the upper-tropospheric EAJS with increasing leads for the demise of WCAR is also higher than that for the onset of WCAR (figure not shown). Pattern correlations between model and observation of the differences in climatological rainfall over west China for these two transitional stages respectively verify the better skill for the ending of WCAR (figure not shown).

5 CONCLUSIONS AND DISCUSSION

The WCAR is characterized by relatively light but incessant and non-ignorable rainfall, following the first peak of rainfall over west China in summer. It has a significant influence on the autumn climate over China. Despite the limited previous effort, the characteristics of

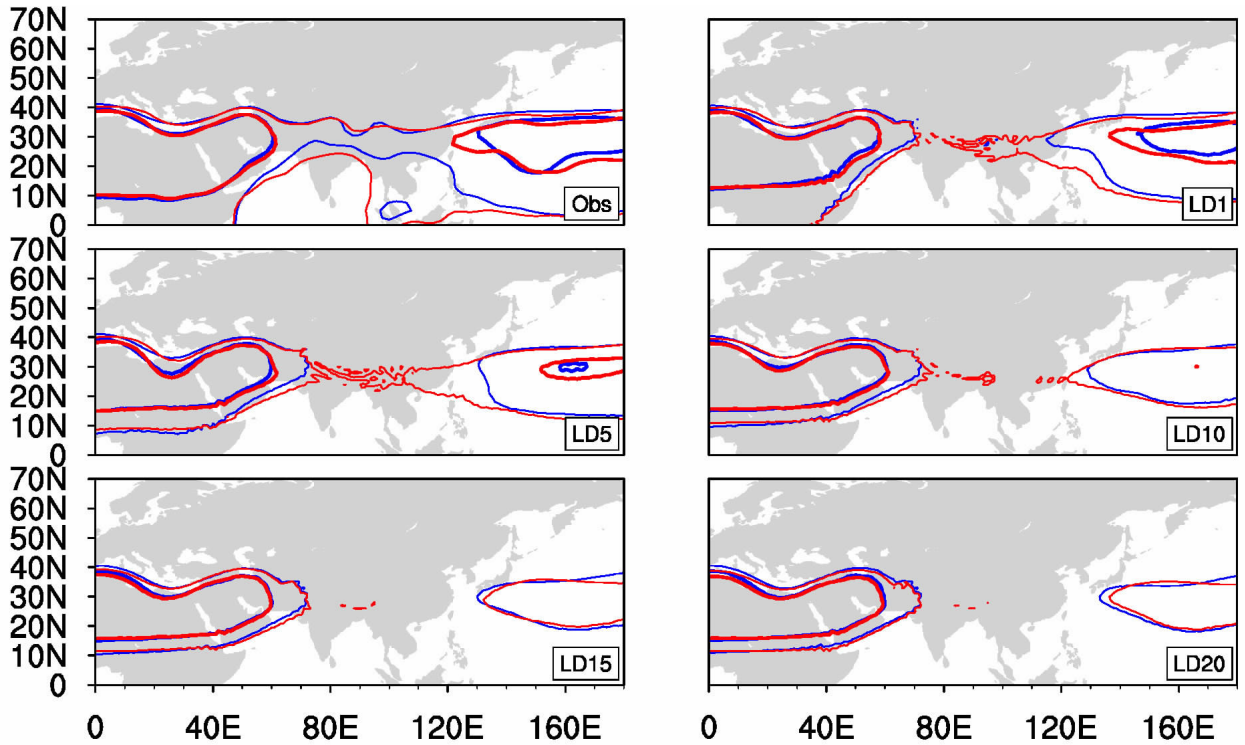

Figure 9. Climatological 3-pentad mean 5880 (thick) and 5860 (thin) geopotential height (contours; meter) during pentads 42-44 (blue) and pentads 46-48 (red) for observation and CFSv2 at LD1, LD5, LD10, LD15, and LD20.

WCAR variations, especially the onset and demise features, and WCAR predictions in dynamical climate forecast systems are seldom investigated. In this study we have used various observational data and the output from the NCEP CFSv2 hindcasts to understand WCAR variations and prediction including the transition features of WCAR onset and demise, the associated atmospheric circulation features, and the skills of dynamical prediction.

The WCAR generally occurs from pentad 46 to pentad 56, with heavy rainfall over the northwestern China and relatively moderate rainfall to the south. Before its onset, the dominant southerly wind changes to southeasterly wind, accompanied by a westward expansion and strengthening of WPSH. This southeasterly flow and the southwesterly monsoon flow transport moisture to west China and lead to enhanced rainfall. On the other hand, during the decay of WCAR, a continental cold high develops and the WPSH weakens and shifts eastward, together with a decay of southwesterly monsoon wind, leading to a decrease in rainfall over west China. Simulating the uneven rainfall distribution of WCAR is a huge challenge for numerical models including the CFSv2. Such challenge comes from the underestimation of the subtropical high. Nevertheless, the CFSv2 well captures several major features including the earlier onset and demise of raining season in northwestern China than in the southern portion. In addition, the model well captures the variation of climatological rainfall during WCAR even after 2 weeks' leads. Due to exaggerated southerly flow, the model exhibits an overestimation of rainfall during the WCAR period. However, this overestimation withers with increasing leads due to the growing underestimated subtropical high. The model can successfully capture the onset and demise dates of WCAR in advance by 5 days and 40 days, respectively. The model shows unrealistically northerly wind anomaly over the lower branch of the Yangtze River, and fails to predict the change in the subtropical high after LD5, contributing to the lower prediction skill for WCAR onset. On the other hand, the transition of atmospheric circulation from the summer pattern to the winter pattern near the end of WCAR is well captured by the CFSv2 up to 40 days, resulting in a preferable prediction for the demise date of WCAR. A better performance of model for the low-level northerly anomaly over the lower branch of the Yangtze River and the movement of the subtropical high could lead to a higher accuracy in predicting WCAR onset.

In this study, we have mainly focused on the climatological features of WCAR and the associated atmospheric circulation. It should be noted that there must be difference in WCAR predictions among different years, as seen from Fig. 10. For example, the years of 2007 and 2014 present outstandingly good skills attaining long leads up to 28 days, while the skill for 2001 is only 6 days. Overall, for most years, the skills of capturing the variability of WCAR drop drastically at the leads around two weeks. The causes and associated features deserve further studies to enhance our understanding and

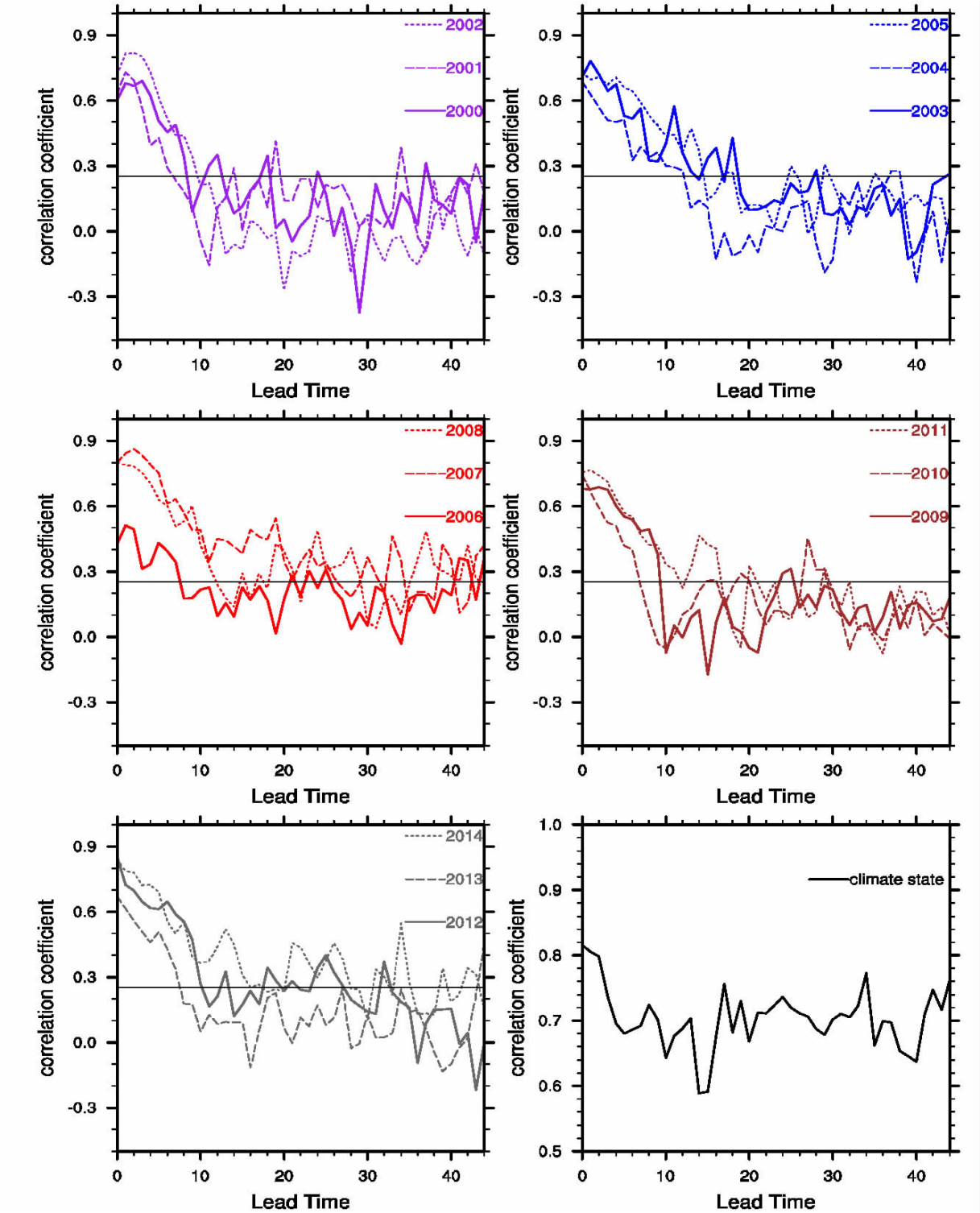

Figure 10. Coefficient of correlation of west China (24.5°-39.5°N, 99.5°-110.5°E) precipitation between observation and CFSv2.

prediction of WCAR.

The years of 2001, 2007, and 2014 are further chosen for a case analysis. According to the area mean bias (blue curves as shown in Fig. 6; but for 2001, 2007, and 2014, figures not shown), overestimations of rainfall are all shown from LD0 to LD40 in the model among the three years in general. The bias of annual mean rainfall suffers from a larger fluctuation with increasing leads in 2001 compared with 2007 and 2014 when the range of biases is closer to that of climatological state shown in Fig. 6. In addition, the onset and demise of WCAR in 2001 also exhibit lower skill in the model. Positive bias of WCAR is more obvious in 2007: the positive bias maintains at a high level of above 1 mm/day with little change from LD0 to LD40. However, in 2001 the positive bias shows a sharper change with increasing leads and is

even replaced by negative values at long leads, associated with the relatively more northward location of the EAJS in the model.

In the model, the location of the EAJS during WCAR is relatively more southward than observed for 2007 while it is comparatively northward for 2001. In observation, the region where U200 exceeds 20 m/s in 2001 is broader, which implies a stronger EAJS during WCAR in 2001 than in 2007 and 2014. The model well pinpoints the location and the magnitude of EAJS during WCAR in the three years but skills drop after LD5. At the middle troposphere, the change to the subtropical high during WCAR can also explain the low skill of WCAR in 2001: the subtropical high exhibits a larger change during WCAR with its western edge extending from 150°E to 90°E in 2001, but from 140°E to 120°E in 2007, and from 120°E to 100°E in 2014, respectively. The strong fluctuation of the subtropical high brings a challenge to forecast the WCAR in 2011. According to the left panel of Fig. 11 (only 2001 is shown), the low-level winds in observation exhibit stronger outbreak and southward invasion of cold air from the north in 2001, compared

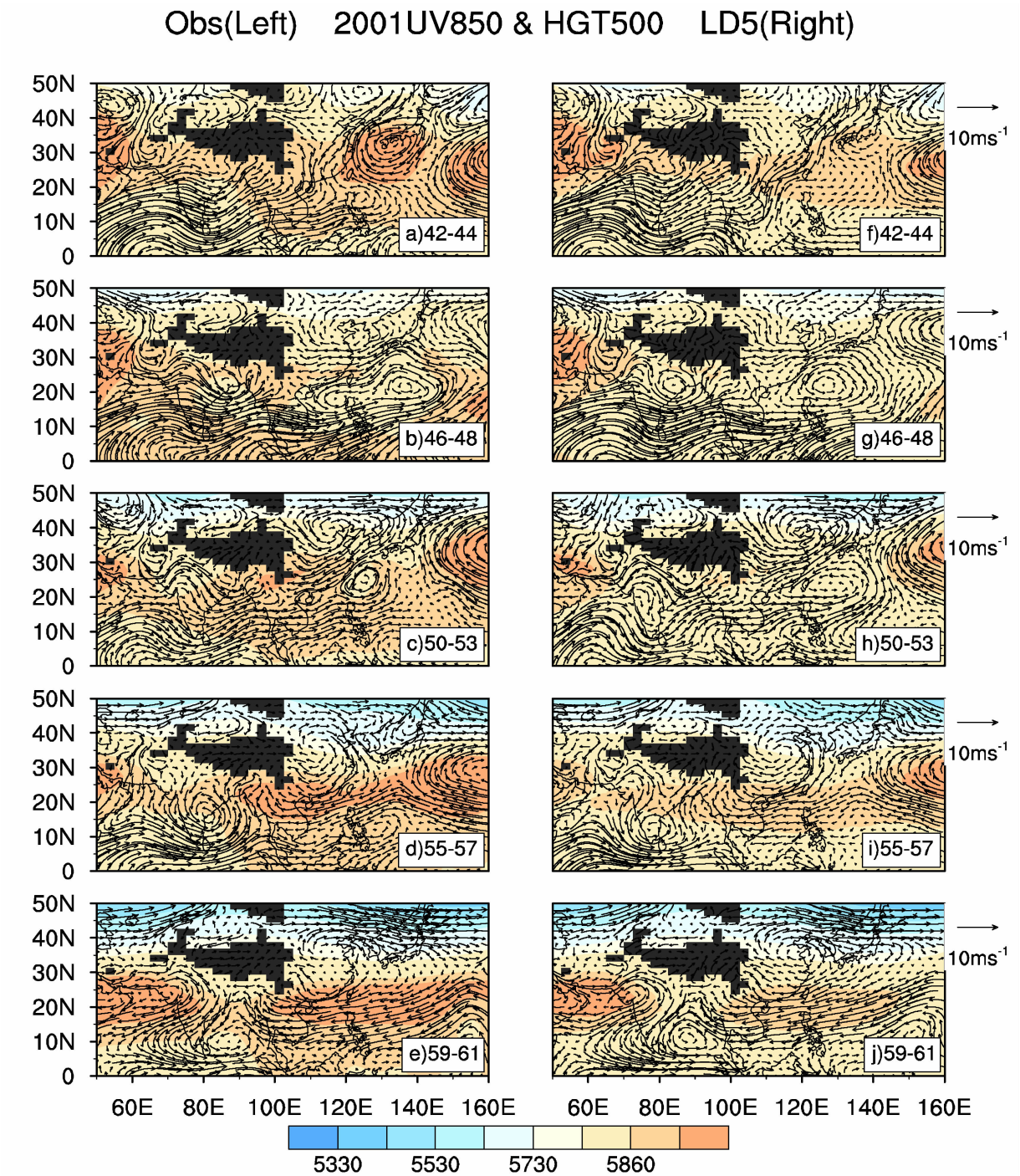

Figure 11. Three-pentad mean 850-hPa winds (vectors; m/s) and 500-hPa geopotential height (shaded areas; meter) in 2001 for observation (left panels) and CFSv2 LD5 (right panels).

with the years of 2007 and 2014. The sharp transformation of low-level circulation in 2001 also makes it harder to capture the related atmospheric circulation features. The difference in UV850 between model and observation during WCAR in 2001 also shows that the model cannot capture the sudden change from southerlies to easterlies after the onset of WCAR when the lead time is longer than 5 days (figures not shown), which is consistent with the result discussed above. In short, the low skill for the WCAR in 2001 is mainly contributed to the high threshold of capturing the related circulation features.

Acknowledgments: The authors thank the two anonymous reviewers who provided helpful comments for improving the overall quality of the paper.

REFERENCES:

[1] ZHANG Bao-kun. Climatic region of Szechwan province [J]. Acta Meteor Sinica, 1941, 17 (Suppl.1): 111-144 (in Chinese).

[2] BAI Hu-zhi, DONG Wen-jie. Climate features and formation causes of autumn rain over southwest China [J]. Plateau Meteor, 2004, 23(6): 884-889 (in Chinese).

[3] YUAN Xu, LIU Xuan-fei. Onset-withdrawal dates of autumn persistent rains over western China and the associated autumn to winter evolution of the atmospheric circulation[J]. Acta Meteor Sinica, 2013, 71(5): 913-924 (in Chinese).

[4] KAO Yu-shie, KUO Chi-yun. On the autumn raining area in China [J]. Acta Meteor Sinica, 1958, 29 (4): 264-273 (in Chinese).

[5] LIANG Jian-hong. The regional and seasonal distribution of autumn rain in west China[J]. Sci Geogra Sinica, 1989, 9(1): 51-59 (in Chinese).

[6] WANG Zun-ya, DING Yi-hui. Climatic characteristics of rainy seasons in China [J]. Chin J Atmos Sci, 2008, 32(1): 1-13 (in Chinese).

[7] YU Ya-xun, WANG Shi-gong, QIAN Zheng-an, et al. Climatic linkages between SHWP position and EASM rainy-belts and-areas in east part of China in summer half year[J]. Plateau Meteor, 2013, 32(5): 1510-1525 (in Chinese).

[8] BAO Yuan-yuan, ABULIMITI L F, WANG X W. Space-time distribution and physical mechanisms of autumn rains in west China in 2001[J]. J Appl Meteor, 2003, 14(2): 215-222 (in Chinese).

[9] CAI Xiang-ning, KANG Zhi-ming, NIU Ruo-yun, et al. Analysis of features and physical mechanisms of 2011 autumn rainfall in west China[J]. Mon Meteor, 2012, 38(7): 828-833 (in Chinese).

[10] LI Ying, LI Wei-jing, AI Wan-xiu, et al. Analysis of autumn rainfall characteristics and its causes in west China in 2011[J]. Adv Met S&T, 2012, 2(3): 27-33 (in Chinese).

[11] LIU Yan-ju, SUN Leng, SUN Cheng-hu, et al. Analysis of anomalies of autumn rain in west China in 2011[J]. Mon Meteor, 2012, 38(4): 456-463 (in Chinese).

[12] WANG Chun-xue, MA Zhen-feng, ZHANG Shun-qian, et al. Establish and analysis of the daily monitoring index for Huaxi autumn rain [J]. Mon Meteor, 2014, 40(8): 957-964 (in Chinese).

[13] HUANG Yan, ZHANG Ren-he, GONG Zhi-qiang, et al. An objectively quantitative division for rainy seasons in China [J]. Acta Meteor Sinica, 2014, 72(6): 1186-1204 (in Chinese).

[14] REN Bing-tan, LI Hui-ying. A preliminary approach to rainy autumns over West China in recent 2000 years [J]. Mon Meteor, 1987, 13(9): 21-24 (in Chinese).

[15] JIANG Zhu-jiang, MA Zhen-feng, LIU Jia, et al. Improved index and climatological characteristics of the autumn rain in western China [J]. Chin J Atmos Sci, 2014, 38(1): 32-44 (in Chinese).

[16] WANG Chun-xue, MA Zhen-feng, WANG Jia-jin, et al. The characteristics of Huaxi autumn rain and its relationship with sea surface temperatures over the equatorial Pacific [J]. Chin J Atmos Sci, 2015, 39(3): 643-652 (in Chinese).

[17] XU Kang, ZHU Cong-wen, WANG Wei-qiang. The cooperative impacts of the El Niño-Southern Oscillation and the Indian Ocean Dipole on the interannual variability of autumn rainfall in China [J]. Int J Climatol, 2016, 36(4): 1987-1999.

[18] FENG Li-wen, GUO Qi-yun. The fluctuation of autumn rain in southwest China [J]. Geogra Res, 1983, 2(1): 74-84 (in Chinese).

[19] ZHAO Shan-shan, ZHANG Qiang, CHEN Yu, et al. Change in autumn precipitation in Weihe and Hanshui river basins [J]. Adv Climate Change Res, 2006, 2(4): 181-183 (in Chinese).

[20] XUE Chun-fang, HOU Wei, ZHAO Jun-hu, et al. The application of ensemble empirical mode decomposition method in multiscale analysis of region precipitation and its response to the climate change [J]. Acta Phys Sin, 2013, 62(10): 504-511 (in Chinese).

[21] XUE Chun-fang, DONG Wen-jie, LI Qing, et al. Climate characteristic and formative cause of autumn rain in Weihe river basin in recent 50 years [J]. Plateau Meteor, 2012, 31 (2): 409-417 (in Chinese).

[22] LUO Xiao, LI Dong-liang, WANG Hui. New evolution features of autumn rainfall in west China and its responses to atmospheric circulation[J]. Plateau Meteor, 2013, 32(4): 1019-1031 (in Chinese).

[23] WANG Chun-xue, MA Zhen-feng, SHAO Peng-cheng, et al. Climate variation of Huaxi autumn rain and the impact factors influencing it [J]. Arid Zone Res, 2015, 32(6): 1113-1121 (in Chinese).

[24] CHEN Zhong-ming, LIU Fu-ming, ZHAO Ping, et al. Relationship between the surface heating fields over Qinghai Xizang Plateau and precipitation of southwest China in autumn[J]. Plateau Meteor, 2001, 20(1): 94-99 (in Chinese).

[25] AI Kai, ZHENG Yi-qun, ZENG Xin-min, et al. Effect of different cloud microphysical parameterization schemes of WFR model on autumn precipitation over west China [J]. J Meteor Environ, 2016, 32(2): 1-10 (in Chinese).

[26] SHAO Jian, DING Yong-hong, ZHAO Guang-ping, et al. Diagnosis and analysis of anomaly of constantly rainy weather over Ningxia province during autumn in 2007 [J]. J Shananxi Meteor, 2009, (1): 18-22 (in Chinese).

[27] HE Min. Long-range forecast and distribution of autumn

rain area in China[J]. Mon Meteor, 1984, (9): 10-13 (in Chinese).

[28] LIU Jia, XU Jin-xia, MA Zhen-feng, et al. Evaluation of flood season prediction in southwest region by the Second-Generation Monthly Dynamic Extended-Range Forecast[J]. Plateau Meteor, 2014, 33(6): 1468-1479 (in Chinese).

[29] PAN Liu-jie, ZHANG Hong-fang, YUAN Yuan, et al. Verification of precipitation forecasting for autumn continuous rainfall by T639 refined grid model in Shaanxi province[J]. J Meteor Envi, 2015, 31(6): 9-17 (in Chinese).

[30] SAHA S, NADIGA S, THIAW C, et al. The NCEP climate forecast system[J]. J Climate, 2006, 19(15): 3483-3517, doi:10.1175/JCLI3812.1.

[31] SAHA S, MOORTHI S, PAN H L, et al. The NCEP climate forecast system reanalysis[J]. Bull Amer Meteor Soc, 2010, 91(8): 1015-1057.

[32] GAO Hui, YANG Song, KUMAR A, et al. Variations of the East Asian Mei-Yu and simulation and prediction by the NCEP climate forecast system [J]. J Climate, 2011, 24 (1): 94-108.

[33] YANG Song, ZHANG Zu-qiang, KOUSKY V E, et al. Simulations and seasonal prediction of the Asian summer monsoon in the NCEP climate forecast system[J]. J Climate, 2008, 21(15): 3755-3775.

[34] LI Yue-qing, YANG Song. A dynamical index for the east Asian winter monsoon[J]. J Climate, 2010, 23(15): 4255-4262.

[35] ZUO Zhi-yan, YANG Song, HU Zeng-Zhen, et al. Predictable patterns and predictive skills of monsoon precipitation in northern hemisphere summer in NCEP CFSv2 reforecasts[J]. Climate Dyn, 2013, 40(11-12): 3071-3088.

[36] KIM Hye-Mi, WEBSTER P J, CURRY J A. Seasonal prediction skill of ECMWF system 4 and NCEP CFSv2 retrospective forecast for the northern hemisphere winter [J]. Climate Dyn, 2012, 39(12): 2957-2973.

[37] JIANG Xing-wen, YANG Song, LI Yue-qing, et al. Seasonal-to-interannual prediction of the Asian summer monsoon in the NCEP climate forecast system version 2 [J]. J Climate, 2013, 26(11): 3708-3727.

[38] WANG Wan-qiu, HUNG Meng-Pai, WEAVER SCOTT J, et al. MJO prediction in the NCEP climate forecast system version 2 [J]. Climate Dyn, 2014, 42(9-10): 2509-2520.

[39] GAO Zong-ting, HU Zeng-Zhen, BHASKAR J, et al. Variability and predictability of northeast China climate during 1948-2012[J]. Climate Dyn, 2014, 43(3-4): 787-804.

[40] ZHAO Si-yu, YANG Song. Dynamical prediction of the early season rainfall over southern China by the NCEP climate forecast system [J]. Wea Forecasting, 2014, 29(6): 1391-1401.

[41] ZHAO Si-yu, YANG Song, DENG Yi, et al. Skills of yearly prediction of the early-season rainfall over southern China by the NCEP climate forecast system[J]. Theor Appl Climatol, 2015, 122(3-4): 743-754.

[42] EK M B, MITCHELL K E, LIN Y, et al. Implementation of Noah land surface model advances in the National Centers for Environmental Prediction operational mesoscale Eta model[J]. J Geophys Res, 2003, 108(D22): 8851, doi: 10.1029/2002JD003296.

[43] GRIFFIES S M, HARRISON M J, PACANOWSKY R C, et al. A technical guide to MOM4 GFDL Ocean Group Technical Report 5[J]. NOAA/GFDL: Princeton, NJ, USA, 2003: 295.

[44] ZHANG Tuan-tuan, YANG Song, JIANG Xing-wen, et al. Sub-seasonal prediction of the maritime continent rainfall of wet-dry transitional seasons in the NCEP climate forecast version 2 [J]. Atmosphere, 2016, 7(2): 28.

[45] ADLER R F, HUFFMAN G J, CHANG A, et al. The version-2 Global Precipitation Climatology Project (GPCP) monthly precipitation analysis (1979-present) [J]. J. Hydrometeor, 2003, 4(6): 1147-1167.

[46] DEE D P, UPPALA S M, SIMMONS A J, et al. The ERA-Interim reanalysis: configuration and performance of the data assimilation system [J]. Quart J Roy Meteor Soc, 2011, 137(656): 553-597.

[47] KALNAY E, KANAMITSU M, KISTLER R, et al. The NCEP/NCAR 40-year reanalysis project[J]. Bull Amer Meteor Soc, 1996, 77(3): 437-471.

[48] YUAN Xu. Temporal and Spatial Characteristics of Autumn Persistent Rainfall Over the Western China and Its Interannual Variation [D]. Nanjing Univ Info Sci Technol, 2013 (in Chinese).

[49] XU Gui-yu, LIN Chun-yu. Survey on the causes and features of autumn rain in western China[J]. Sci Meteor Sinica, 1994, 14(2): 149-154 (in Chinese).

[50] YANG Song, LAUI K M, KIM K M. Variations of the East Asian jet stream and Asian-Pacific-American winter climate anomalies [J]. J Climate, 2002, 15(3): 306-325.

[51] YEH Tu-cheng, DAO Shih-yen, LI Mei-tsiun. The abrupt change of circulation over northern hemisphere during June and October[J]. Acta Meteor Sinica, 1958, 29(4): 249-263 (in Chinese).

[52] CHEN Shao-yong, XIA Quan, GUO Jun-tin, et al. Relationship analysis between September precipitation in western China and 700 hPa wind field in East Asia [J]. Sci Cold Arid Reg, 2011, 3(5): 419-425.

[53] ZHANG Nan, WANG Xiao, CHENG Jia-he. Study of transport and budget of water vapor resources in central China[J]. Meteor Environ Sci, 2011, 34(2): 25-30 (in Chinese).

Citation: DONG Shao-rou, YANG Song, ZHANG Tuan-tuan, et al. Dynamical prediction of west China autumn rainfall by the NCEP climate forecast system [J]. J Trop Meteor, 2019, 25(1): 114-128.